





Insulin receptor orchestrates kidney antibacterial defenses

Laura Schwartz^{a,b} , Aaron Simoni^a , Pearly Yan^{c,d} , Kristin Salamon^a, Altan Turkoglu^d, Gabriela Vasquez Martinez^a, Diana Zepeda-Orozco^{a,b}, Tad Eichler^a, Xin Wang^a , and John David Spencer^{a,b,1} 

Edited by Scott Hultgren, Washington University School of Medicine in St. Louis, St. Louis, MO; received January 15, 2024; accepted June 6, 2024

Urinary tract infection (UTI) commonly afflicts people with diabetes. This augmented infection risk is partly due to deregulated insulin receptor (IR) signaling in the kidney collecting duct. The collecting duct is composed of intercalated cells (ICs) and principal cells (PCs). Evidence suggests that ICs contribute to UTI defenses. Here, we interrogate how IR deletion in ICs impacts antibacterial defenses against uropathogenic *Escherichia coli*. We also explore how IR deletion affects immune responses in neighboring PCs with intact IR expression. To accomplish this objective, we profile the transcriptomes of IC and PC populations enriched from kidneys of wild-type and IC-specific IR knock-out mice that have increased UTI susceptibility. Transcriptomic analysis demonstrates that IR deletion suppresses IC-integrated stress responses and innate immune defenses. To define how IR shapes these immune defenses, we employ murine and human kidney cultures. When challenged with bacteria, murine ICs and human kidney cells with deregulated IR signaling cannot engage central components of the integrated stress response—including activating transcriptional factor 4 (ATF4). Silencing ATF4 impairs NFκB activation and promotes infection. In turn, NFκB silencing augments infection and suppresses antimicrobial peptide expression. In diabetic mice and people with diabetes, collecting duct cells show reduced IR expression, impaired integrated stress response engagement, and compromised immunity. Collectively, these translational data illustrate how IR orchestrates collecting duct antibacterial responses and the communication between ICs and PCs.

pyelonephritis | insulin receptor | collecting duct | intercalated cells | NF-κB

With diabetes, urinary tract infection (UTI) is frequent, severe, and associated with worse outcomes. UTI complications, such as kidney scarring, kidney injury, emphysematous pyelonephritis, and kidney abscess formation, are more common with diabetes (1–5). Historically, hyperglycemia is considered the principal UTI driver by promoting bacterial replication and attenuating immune responses. Newer evidence suggests that insulin resistance, which develops prior to hyperglycemia, is a sentinel UTI risk factor (6). Insulin resistance is defined by compromised insulin receptor (IR) signaling (7). In the kidney, IR is expressed throughout the glomerulus, nephron, and collecting duct (8). Our research team has demonstrated that IR deletion in the distal nephron and collecting duct heightens UTI susceptibility. Furthermore, we have shown that IR deletion in intercalated cells (ICs) of the collecting duct increases UTI susceptibility by suppressing antimicrobial peptide (AMP) production (6). Given these findings, a deeper exploration into IR-mediated antibacterial responses in the kidney is needed, as these processes could potentially be leveraged to reduce UTI and its associated complications.

Uropathogenic *Escherichia coli* (UPEC) is the predominant UTI-causing pathogen. During UTI, UPEC can ascend into the kidney and cause pyelonephritis—a severe and occasionally life-threatening infection (9). When reaching the kidney, UPEC invades the collecting duct where they adhere to the luminal surface of ICs (10, 11). ICs have a vital role in UTI defense by acidifying the urine to impede pathogen replication, activating pattern recognition receptors and inflammatory cytokines, secreting AMPs, and phagocytosing UPEC to promote pathogen clearance (9–16). In addition to ICs, collecting ducts are composed of principal cells (PCs). The role of PCs in UTI defense is less defined.

Considering the pivotal role ICs play in UTI prevention and our previous discoveries indicating that IR shapes their antibacterial defenses, the primary objective of this study is to comprehensively assess the contribution of IR signaling to the antibacterial capacity of ICs. The secondary objective is to interrogate how IC-specific IR deletion impacts neighboring PCs with intact IR expression. To do so, we delete IR in ICs and enrich ICs and PCs from wild-type (WT) and IR knock-out (IRKO) mouse kidneys using fluorescent activated cell sorting (FACS). We then perform RNA sequencing (RNA-seq) and compare mRNA expression in four groups: WT ICs, IRKO ICs, PCs from WT collecting ducts, and PCs from IRKO collecting ducts. In doing so, we find that ICs require IR to engage

Significance

It is unclear why people with diabetes frequently develop urinary tract infection (UTI). In this study, we investigate how insulin receptor (IR) signaling shapes kidney antibacterial defenses that prevent infection. Our primary outcomes show that deregulated IR signaling increases UTI susceptibility by inactivating essential integrated stress responses and immune pathways that prevent infection. The translational significance of these findings is validated by showing that kidneys from people with diabetes have suppressed expression of IR and its downstream immune targets. Ultimately, these findings may establish a foundation to target IR signaling nodes to improve outcomes of diabetes-associated infections.

Author affiliations: ^aThe Kidney and Urinary Tract Center, Abigail Wexner Research Institute at Nationwide Children's, Columbus, OH 43205; ^bDivision of Nephrology and Hypertension, Department of Pediatrics, Nationwide Children's, Columbus, OH 43205; ^cComprehensive Cancer Center, Arthur G. James Cancer Hospital and Richard J. Solove Research Institute, The Ohio State University Wexner Medical Center, Columbus, OH 43210; and ^dDepartment of Internal Medicine, The Ohio State University College of Medicine, Columbus, OH 43210

Author contributions: L.S., T.E., X.W., and J.D.S. designed research; L.S., A.S., P.Y., K.S., A.T., G.V.M., D.Z.-O., T.E., and J.D.S. performed research; P.Y. and D.Z.-O. contributed new reagents/analytic tools; L.S., A.S., X.W., and J.D.S. analyzed data; and L.S. and J.D.S. wrote the paper.

The authors declare no competing interest.

This article is a PNAS Direct Submission.

Copyright © 2024 the Author(s). Published by PNAS. This article is distributed under [Creative Commons Attribution-NonCommercial-NoDerivatives License 4.0 \(CC BY-NC-ND\)](https://creativecommons.org/licenses/by-nc-nd/4.0/).

¹To whom correspondence may be addressed. Email: john.spencer@nationwidechildrens.org.

This article contains supporting information online at <https://www.pnas.org/lookup/suppl/doi:10.1073/pnas.2400666121/-/DCSupplemental>.

Published July 8, 2024.

integrated stress responses that activate NF κ B and downstream UTI defenses. We also report that IR deletion in ICs reprograms IC–PC communication and suppresses NF κ B in neighboring PCs. We correlate these findings using diabetic mice and kidney single-cell RNA-seq (scRNA-seq) data available from people with diabetes. These complementary and translational models elucidate a key role for IR in orchestrating collecting duct defenses that prevent UTI.

Results

Systemic IR Inhibition Increases UPEC Susceptibility. To interrogate whether IR impacts kidney UPEC susceptibility, we treated female C3H/HeOuj mice with OSI-906, an IR/insulin-like growth factor 1 receptor (IGF1R) inhibitor, and infected them with UPEC (Fig. 1A) (17). We selected C3H/HeOuj mice because they have a higher propensity to develop pyelonephritis compared to C57BL/6 mice (18, 19). Mice treated with OSI-906 exhibited suppressed kidney IR/IGF1R activity, increased blood glucose concentrations, and glucosuria—indicative of successful IR inhibition (Fig. 1B/C). After transurethral UPEC infection, all mice exhibited kidney bacterial burden. Mice receiving OSI-906 had significantly higher UPEC titers in their kidneys, suggesting that suppressed IR activity is a UTI risk factor (Fig. 1D).

IR Deletion in ICs Increases UPEC Susceptibility. To assess whether IC-specific IR signaling influences kidney UPEC susceptibility, we selectively deleted IR in ICs by crossing homozygous *Insr^{fl/fl}* mice with V-ATPase-Cre mice that express Cre-recombinase under the *Atp6v1b1* promoter (Fig. 2A) (20). All mouse strains are on a C57BL/6J background. Available scRNA-seq data show that *Atp6v1b1* has robust expression in C57BL/6J ICs and limited expression in other kidney cells (SI Appendix, Fig. S1) (21). Throughout this manuscript, mice with IR deletion are referenced as IRKO. Our published data show that IRKO mice have normal phenotypes, kidney histopathology, and glucose regulation. Our data also show that IRKO mice have increased urinary and bladder UPEC titers following transurethral UTI (6).

Although we previously reported higher kidney UPEC titers following transurethral UTI, the limited number of measured kidney UPEC colonies prevented us from forming definitive conclusions about the significance of IR in kidney antibacterial defense (6). This reflects the inherent resistance of C57BL/6J mice to pyelonephritis following transurethral UTI (18, 19). To address this constraint, we infected control (IRflox) and IRKO mice by direct bladder inoculation to promote UPEC ascension to the kidneys (22). Prior to infection, IRKO and IRflox mice exhibited comparable blood glucose concentrations and no evidence of glucosuria (Fig. 2B). Twenty-four hours after infection, IRKO mice had greater kidney UPEC titers, indicating that IR expression in ICs is important for kidney antibacterial defenses (Fig. 2C).

Enrichment and RNA-seq Profiling of IC and PC Populations. To examine the impact of IR deletion on IC immune defenses and assess whether IR deletion affects neighboring PCs that retain IR expression, we used established methods to FACS-enrich tdT-expressing ICs and FITC-conjugated *Dolichos biflorus* agglutinin (DBA) lectin labeled PCs (Fig. 3A/B and SI Appendix, Figs. S1 and S2) (6, 23). VATPase-tdT mice were utilized as WT controls for FACS. Following transurethral UTI, they exhibit comparable bladder and kidney burden to IRflox controls and less bacterial burden compared to IRKO mice (SI Appendix, Fig. S3). Following FACS enrichment, Cre recombination was detected in IRKO ICs but not in PCs (Fig. 3C). For simplicity, PCs isolated from IRKO mice are referred to as IRKO PCs, acknowledging that they express IR. *Insr* transcript expression was suppressed in IRKO IC populations but comparable in PC populations, providing supporting evidence of IC-selective Cre recombination (Fig. 3D and Dataset S1).

Limiting-cell RNA-seq was performed on IC and PC populations from WT and IRKO kidneys. Principal component analysis shows that IC and PC samples cluster into distinct groups with the largest variance occurring between cell types on principal component 1 (IC vs. PC) and the secondary axis of variance separating samples by genotype (WT vs. IRKO, Fig. 3E). Genes known to be expressed by ICs and PCs and gene ontology analysis confirm

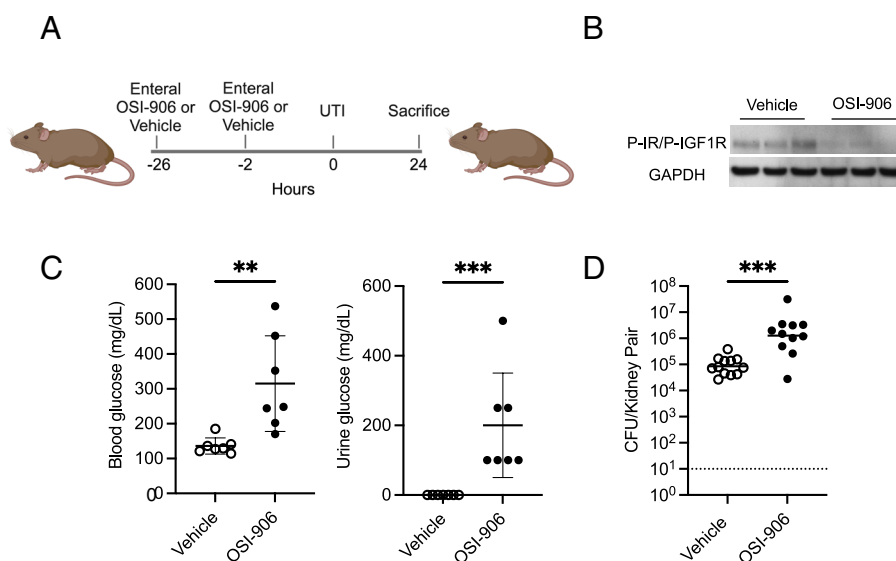


Fig. 1. Systemic IR inhibition increases kidney bacterial burden. (A) Schematic showing how female C3H/HeOuj were enterally administered vehicle or OSI-906 (60 mg/kg) prior to transurethral UPEC infection (strain CFT073). (B) Representative western blot probed for P-IR/IGF1R and GAPDH in kidneys from vehicle- or OSI-906-treated female mice. Each lane depicts protein expression in a separate mouse kidney. (C) Blood (Left) and urine (Right) glucose concentrations measured in a subset of mice subjected to transurethral UTI. Each point depicts glucose measurement in a unique mouse ($n = 7$ mice/cohort). Graphs show the mean values and SD. (D) Kidney UPEC titers enumerated 24 h after transurethral infection. Each point shows mean kidney pair UPEC burden from a separate mouse ($n = 11$ to 12 mice/cohort). The solid horizontal lines indicate the geometric means. The dotted horizontal line indicates the limit of detection. (C/D) Asterisks denote significance for the indicated pairwise comparison (Mann-Whitney U test). ** $P < 0.01$ and *** $P < 0.001$.

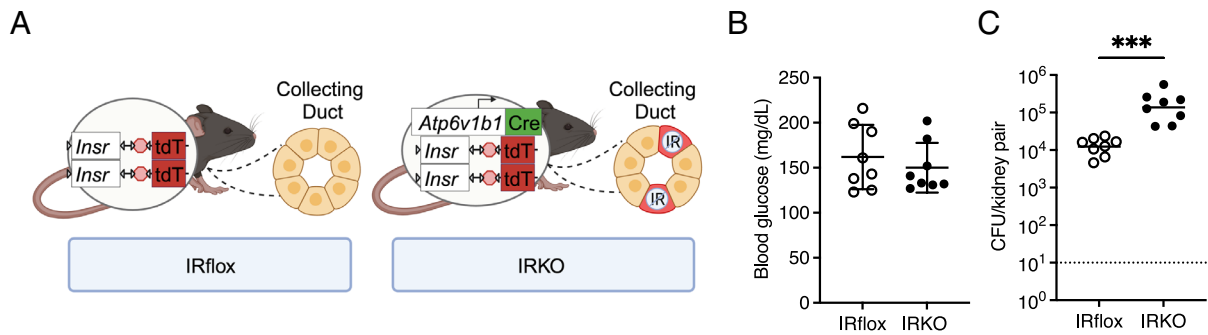


Fig. 2. IR deletion in ICs increases kidney bacterial burden. (A) Schematic of the breeding strategy to delete IR in murine ICs. (B) Blood glucose concentrations measured in IRflox and IRKO mice. Each point depicts the glucose measurement in a unique mouse 24 h after UTI. Graphs show the mean values and SD. (C) Kidney UPEC burden enumerated 24 h after direct bladder infection in IRflox and IRKO mice. Each point shows mean kidney pair UPEC burden from a separate mouse ($n = 8$ mice/cohort). The solid horizontal lines indicate the geometric means. The dotted horizontal line indicates the limit of detection. Asterisks denote significance for the indicated pairwise comparison (Mann-Whitney U test). *** $P < 0.001$.

enrichment of unique IC and PC populations (Fig. 3F and SI Appendix, Fig. S4). Examination of RNA-seq data revealed no differences in the expression of established IC- and PC-specific

genes between WT and IRKO mice (Fig. 3F). These findings were further validated in an additional set of FACS-enriched ICs and PCs through qRT-PCR (SI Appendix, Fig. S5). These findings

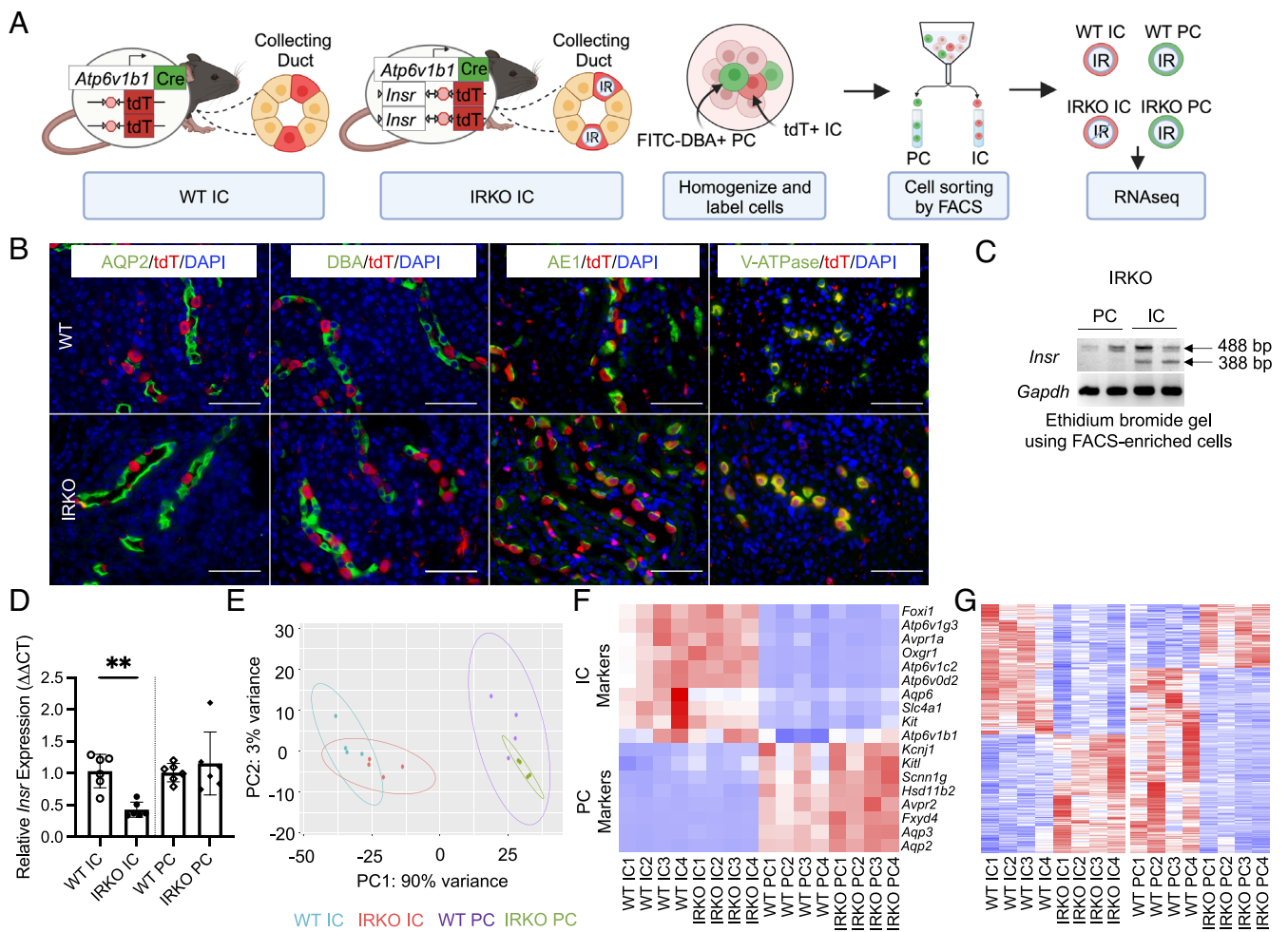


Fig. 3. Enrichment of ICs and PCs yields populations with unique expression signatures. (A) Schematic of V-ATPase-tet (WT) and V-ATPase-IRKO-tet (IRKO) mice and the approach to enrich IC and PC populations using FACS. (B) Immunofluorescent staining of kidney sections from WT (top row) and IRKO mice (bottom row) showing tet expression in ICs (red) does not colocalize with aquaporin 2 (AQP2, green) or DBA labeled PCs (green). Tdt colocalizes with IC-specific proteins AE1 and V-ATPase V1B1 (green). Nuclei are labeled with DAPI (blue). Magnification 60X. (Scale bars, 50 μ m.) (C) Representative ethidium bromide agarose gel using FACS-enriched IRKO PCs and ICs shows a 488 base pair PCR product indicative of the IRflox allele in PC and IC populations and a 388 base pair product indicative of *Insr* deletion in IC populations. *Gapdh* served as a loading control. (D) Relative *Insr* mRNA transcript expression measured by qRT-PCR in FACS-enriched IC and PC populations from WT and IRKO mice. Graphs show the mean expression and SEM. The asterisk marks significance between genotypes ($n = 6$ samples/genotype; Mann-Whitney). ** $P < 0.01$. (E) Principal component analysis showing linear dimensionality reduction in FACS-enriched IC and PC populations. Each point represents IC and PC populations enriched from a different mouse and the 95% confidence ellipses are graphed. (F) Heatmap of established IC and PC marker genes in enriched IC and PC populations from WT and IRKO mice. (G) Heatmap of the 1,000 most differentially expressed genes in ICs and PCs from WT and IRKO mice. (F and G) Columns are individual mice and rows are specific genes.

confirm the enrichment and IC and PC populations and suggest that IR deletion does not impact the expression IC- and PC-specific markers.

A total of 1,794 differentially expressed genes with false discovery rate < 0.05 were identified between WT and IRKO ICs and 650 differentially expressed genes were identified between WT and IRKO PCs. The relative expression of the top 1,000 differentially expressed genes in ICs and PCs is shown (Fig. 3G). These results demonstrate that *Insr* deletion in ICs shifts gene expression in both ICs and PCs.

IR Deletion Suppresses IC-Integrated Stress Responses and Immunity. To assess how IR shapes IC transcriptomes, we performed a pathway enrichment analysis on WT and IRKO ICs. This analysis shows that seven of the ten most enriched canonical pathways are down-regulated in IRKO ICs. These pathways are involved in the integrated stress response and innate immunity (Fig. 4A). In line with the canonical pathways, a transcription factor analysis identified suppressed transcription factor activity in IRKO ICs involved in immune and inflammatory responses—including NFκB genes, Regulatory Factor X (RFX) genes, *Spi1*, and *Cebpb* (Fig. 4B). Similarly, immune gene ontology terms and proinflammatory cytokines were suppressed in IRKO ICs compared to WT ICs (Fig. 4C and *SI Appendix, Table S1*). These analyses imply IR deletion suppresses IC immunity.

IR Deletion Dampens IC Antibacterial Defenses to Facilitate UPEC Infection. Because ICs and PCs comprise a small percentage of the kidney’s cellular population, it can be challenging to assess their individual antibacterial responses. To overcome this limitation, we cultured FACS-enriched ICs and PCs. Characterization of low-passage cultured ICs and PCs confirms Cre-mediated

recombination in IRKO ICs but not in WT IC or PC populations; restricted Tdt expression to ICs; and preservation of IC- and PC-specific marker genes (*SI Appendix, Fig. S6*).

To confirm that IR deletion augments UPEC susceptibility in vitro, we challenged confluent WT and IRKO ICs with UPEC. Following bacterial challenge, the percentage of UPEC attaching to or invading IRKO ICs was significantly greater than WT ICs (Fig. 4D). To validate this finding, we inhibited IR in human kidney medullary epithelial cells with OSI-906 and challenged them with UPEC. Compared to vehicle-treated cells, the percentage of UPEC infecting OSI-906-treated cells was significantly greater (Fig. 4E). These results mirror our in vivo findings, suggesting that this in vitro approach is sufficient to interrogate immune responses in WT and IRKO cells.

To gauge the consequences of IR deletion on IC antibacterial responses during infection, we profiled the expression of antimicrobial response genes in UPEC-challenged ICs. Of the 84 genes profiled, 67 genes were down-regulated in IRKO ICs compared to WT ICs (*SI Appendix, Table S2*). Protein–protein interactions and signal enrichment analyses on these down-regulated genes identified NFκB as a central host defense node that fails to respond to UPEC, insinuating that IR deletion weakens NFκB-mediated immune defenses (Fig. 4F).

Integrated Stress Responses Engage NFκB and Prevent UPEC Infection. EIF2 signaling, the top pathway predicted to be suppressed in IRKO ICs (Fig. 4A), regulates the integrated stress response. When activated, the eukaryotic initiation factor 2 (eIF2) α-subunit promotes ATF4 translation. Studies suggest that ATF4 regulates canonical NFκB signaling (*SI Appendix, Fig. S7*)—the top transcription factor predicted to be suppressed with IR deletion (Fig. 4B) (24–27). To test whether IR impacts ATF4 or NFκB activity in ICs, we transurethrally

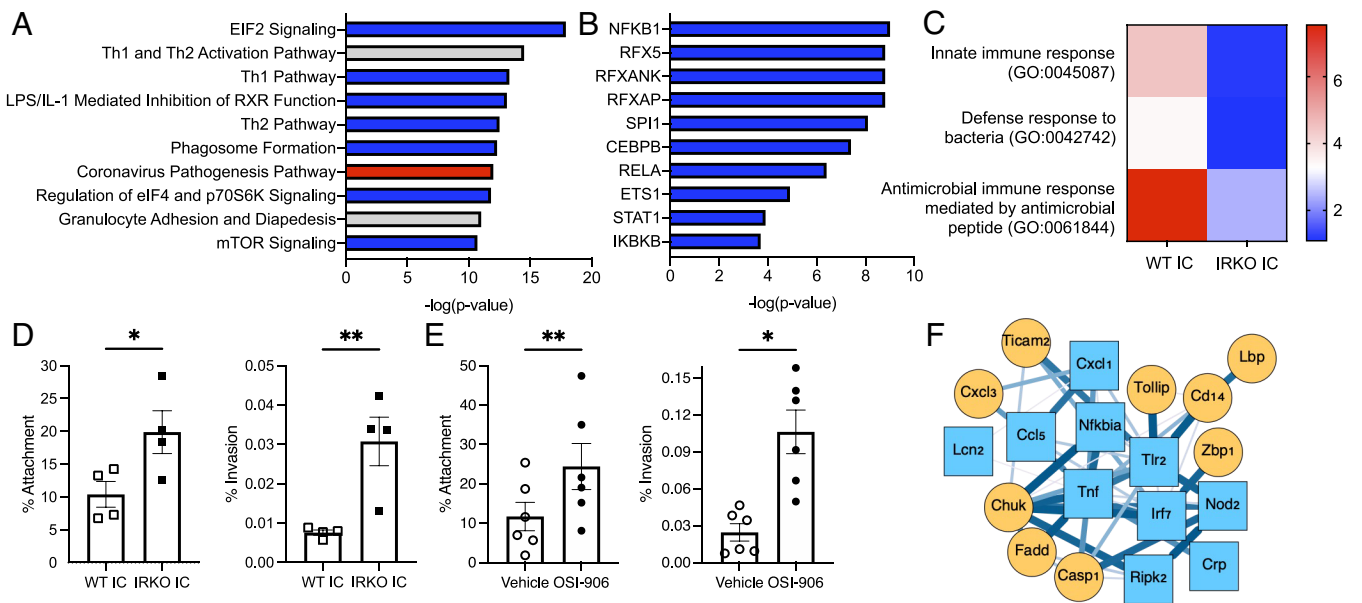


Fig. 4. IR deletion in ICs suppresses integrated stress responses, NFκB signaling, and innate immune defenses. (A) Ingenuity pathway analysis showing the predicted canonical pathways that are suppressed (blue bars) or activated (red bars) in IRKO ICs compared to WT ICs ($|Z\text{-score}| > 2$). Gray bars indicate that no prediction could be made on pathway activation or suppression. (B) Metascape TRRUST analysis identifies transcription factors regulating differential gene expression in IRKO ICs. Blue bars indicate the transcription factors whose activity is predicted to be suppressed. (C) Heatmap showing changes in innate immune gene ontology term enrichment in IRKO ICs compared to WT ICs. (A–C) RNA-seq data analyses were performed on ICs enriched from WT and IRKO mouse kidneys as shown in Fig. 3. (D/E) Cultured WT and IRKO ICs (D) were challenged with UPEC. (E) Human medullary kidney cells were pretreated with OSI-906 (1 μM) and then challenged with UPEC. Shown is the percentage of bacteria attaching to the cellular surface (Left) or invading the cells (Right). Graphs show the mean and SEM. Results are from four (D) or six (E) independent experiments performed in triplicate. Asterisks denote significant *P*-values for the pairwise comparison (Student’s *t* test). **P* < 0.05 and ***P* < 0.01. (F) WT and IRKO ICs were challenged with UPEC for 60 min. Antibacterial response RT-PCR arrays were performed (*n* = 4 samples/genotype) and a protein–protein interaction network was generated with STRING using the significantly suppressed genes identified by the arrays in *SI Appendix, Table S2*. Nodes represent gene products and edges indicate functional or physical interactions. Edge width corresponds to experimentally determined interaction score. Blue square nodes indicate gene targets of NFκB, and yellow circle nodes depict genes that have not been identified as targets of NFκB.

infected IRKO and IRflox mice with UPEC and enriched their ICs using MACS. Due to the inherent variability with in vivo UTI models, we opted for MACS methodology, as experimental groups could be processed simultaneously compared to individually with FACS. Following UTI, we detected suppressed ATF4 and NFkB protein expression in IRKO ICs (Fig. 5A). Similarly, we observed reduced ATF4 and NFkB p65 in UPEC-infected cultured IRKO ICs and OSI-906-treated human kidney cells—indicating that IR is necessary to fully engage ATF4 and NFkB (Fig. 5B/C and SI Appendix, Fig. S8).

To determine whether ATF4 is necessary for NFkB activity, murine ICs and human kidney cells were transfected with an ATF4 or control small interfering RNA (siRNA) pool and challenged with UPEC. With ATF4 silencing, NFkB activation was suppressed (Fig. 5D/E and SI Appendix, Fig. S8). To assess whether ATF4 is sufficient to activate NFkB, we stressed murine ICs with salubrinal and tunicamycin (28, 29). Both agents augmented ATF4 and NFkB (SI Appendix, Fig. S9). Similarly, when we transiently transfected human kidney epithelial cells with a plasmid that constitutively drives ATF4 overexpression, western

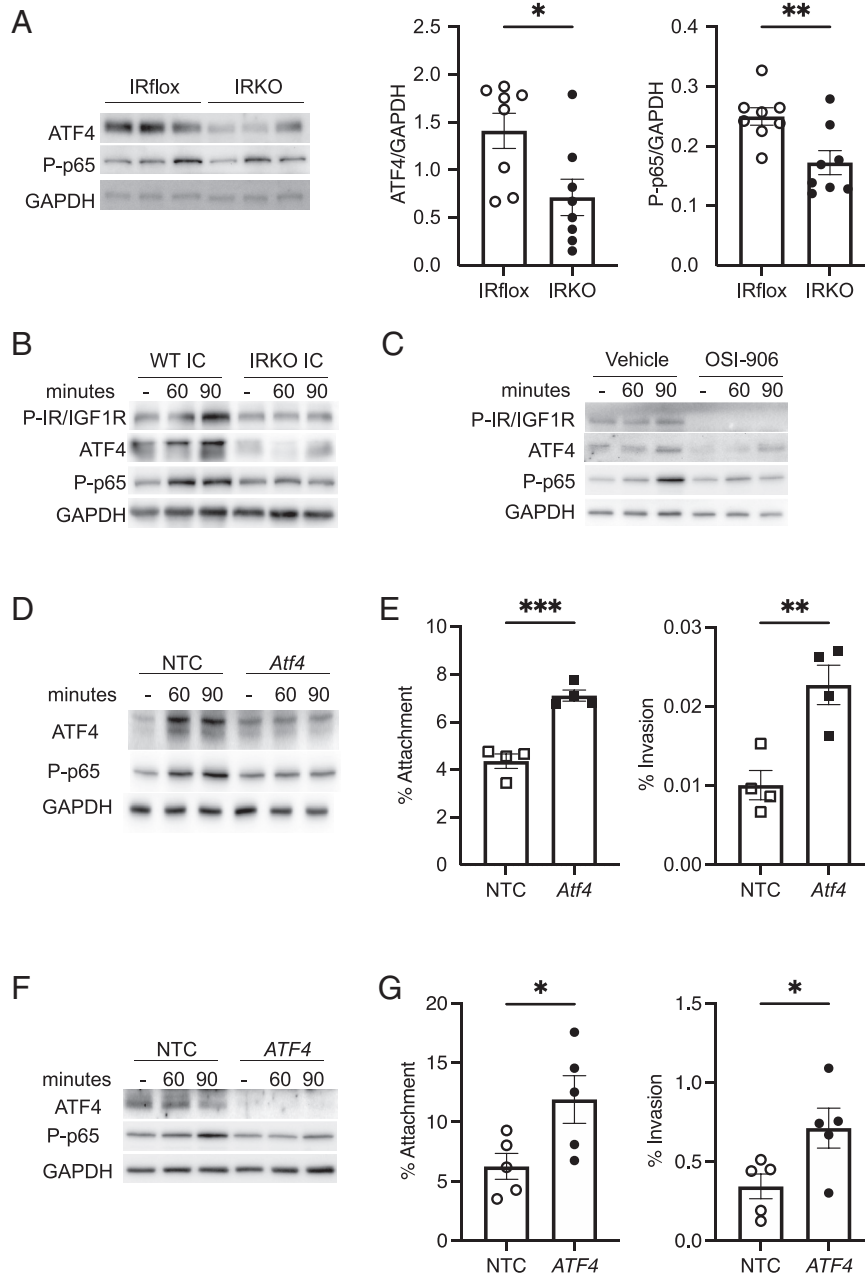


Fig. 5. IR deletion or inhibition suppresses ATF4 and NFkB signaling. (A) Female IRKO and IRflox control mice were transurethraly infected with UPEC. Six hours after infection, ICs were enriched by MACS. Western blot (Left) showing that NFkB and ATF4 are suppressed in IRKO ICs. Each lane depicts ICs enriched from an individual mouse. This experiment was performed twice with 3 to 5 mice/genotype. Densitometry (Right) showing relative abundance of P-p65 NFkB (ser536) and ATF4 normalized to GAPDH from all mice subjected to UTI ($n = 8$ /genotype). Graphs show the mean and SEM. (B/C) Cultured WT and IRKO ICs (B) were challenged with CFT073. (C) Human medullary kidney cells were pretreated with OSI-906 (1 μ M) and then challenged with UPEC. (B/C) Representative western blots showing P-IR/IGF1R, ATF4, P-p65 NFkB (ser536), and GAPDH expression. (D-G) Murine ICs (D/E) or human medullary kidney cells (F/G) were transiently transfected with an ATF4 or a nontargeting control (NTC) siRNA pool. (D/F) Representative western blots showing ATF4, P-p65 NFkB (ser536), and GAPDH expression. (E/G) Murine ICs (E) or human medullary kidney cells (G) were challenged with UPEC. Shown is the percentage of bacteria attaching to the cellular surface (Left) or invading the cells (Right). Graphs show the mean and SEM. Results are from four or five independent experiments performed in quadruplicate ($n = 4$ to 5). (A, E, and G) Asterisks denote significant P -values for the pairwise comparison (Student's t test). * $P < 0.05$, ** $P < 0.01$, and *** $P < 0.001$. (B–D and F) Densitometry was performed to measure relative target abundance from three independent experiments and is shown in SI Appendix, Fig. S8.

blot shows that ATF4 overexpressing cells have increased NFκB activity (*SI Appendix, Fig. S9*). To investigate whether ATF4 impacts UTI, murine ICs and human kidney cells were transfected with an ATF4 or control siRNA pool and challenged with UPEC. ATF4 silencing augmented the percentage of UPEC adhering to or invading the cells (Fig. 5 *E/G*). These experiments establish ATF4-NFκB as a critical node in UTI defense that is impaired with deregulated IR signaling.

NFκB Protects the Kidney from UPEC by Activating AMPs. We next turned our attention to NFκB and evaluated its contributions to kidney antibacterial defense. UPEC attachment and invasion increased when NFκB was silenced in mouse ICs and human kidney cells (Fig. 6 *A–D*). Because our transcriptomic analyses demonstrate AMPs are suppressed in IRKO ICs (Fig. 4*C* and *SI Appendix, Table S2*), we investigated whether NFκB impacts their expression in infected human kidney cells. With *NFKB1* silencing, we observed suppressed *LCN2*, *RNASE4*, and *RNASE7* expression (Fig. 6*E*). To validate the role of NFκB in regulating

AMP expression, we performed ChIP to localize NFκB to their promoters. In noninfected cells, we observed weak NFκB p65 binding at the *LCN2*, *RNASE4*, and *RNASE7* promoters. In infected cells, we observed increased NFκB p65 binding (Fig. 6*F*). These data suggest that NFκB serves as an essential transcription factor facilitating AMP expression.

IR Deletion in ICs Impacts PC Transcriptomes. To determine how IR deletion in ICs impacts neighboring PCs, we performed pathway enrichment analysis on differentially expressed genes from PCs enriched from WT and IRKO kidneys. This analysis predicted five of the ten most enriched canonical pathways are down-regulated in PCs from IRKO mice. Like ICs, these pathways are involved in immune responses (Fig. 7*A* and *SI Appendix, Table S1*). Transcription factor analysis identified suppressed NFκB target gene expression in IRKO PCs (Fig. 7*B*). To assess whether these changes impact NFκB responses to infection, we challenged PCs from WT and IRKO mice with UPEC. Following bacterial challenge, NFκB activity was suppressed in IRKO PCs

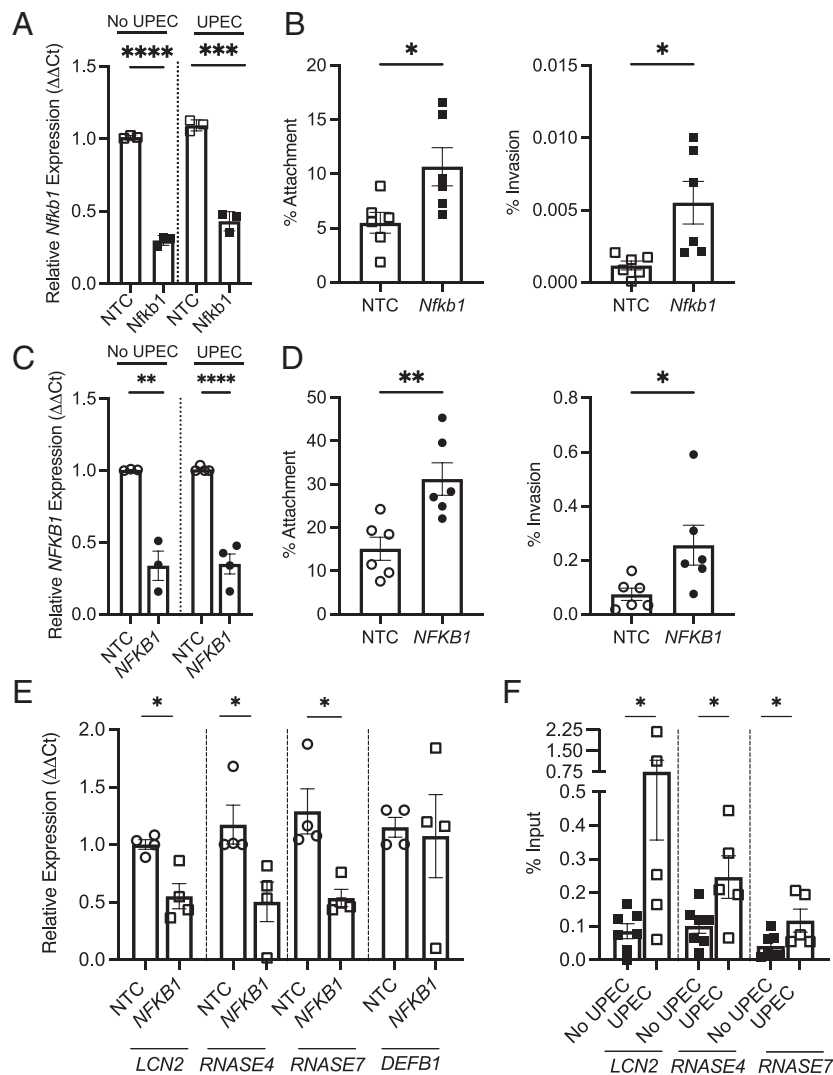


Fig. 6. Silencing NFκB promotes UPEC infection and suppresses AMP expression. (*A/B*) Cultured murine ICs and (*C/D*) human kidney medullary epithelial cells were transiently transfected with a NFκB or nontargeting control (NTC) siRNA pool and challenged with UPEC. (*A/C*) qRT-PCR confirms NFκB silencing in noninfected and UPEC-infected cells. (*B/D*) Shown is the percentage of bacteria attaching to the cellular surface (*Left*) or invading the cells (*Right*). Graphs show the mean and SEM from six independent experiments performed in triplicate ($n = 6$). (*E*) qRT-PCR was performed to assess *LCN2*, *RNASE4*, *RNASE7*, and *DEFB1* transcript expression in UPEC-infected human medullary epithelial cells transfected with a *NFKB1* or NTC siRNA pool. Graphs show the mean expression and SEM from four independent experiments. (*F*) Chromatin immunoprecipitation was performed using noninfected and UPEC-challenged human kidney medullary epithelial cells. Binding of P65 NFκB to the promoters of *LCN2*, *RNASE4*, and *RNASE7* was assessed by qPCR with immunoprecipitated DNA using primers specific to promoter regions of respective genes. Asterisks denote significant P values for the pairwise comparison (Student's t test). * $P < 0.05$, ** $P < 0.01$, *** $P < 0.001$, and **** $P < 0.0001$.

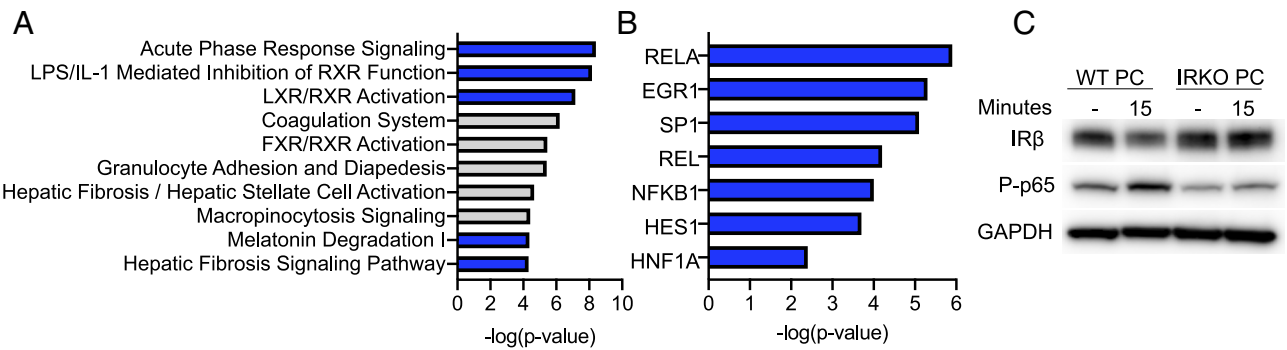


Fig. 7. IR deletion in ICs suppresses immune responses in PCs. (A) Ingenuity pathway analysis revealing the predicted canonical pathways that are suppressed (blue bars) in IRKO PCs compared to WT PCs ($|Z\text{-score}| > 2$). Gray bars highlight no prediction could be made on pathway activation or suppression. (B) Metascape TRRUST prediction of transcription factors regulating the suppressed genes in IRKO PCs. Blue bars show the transcription factors whose activity is predicted to be suppressed. (A/B) Analyses of RNA-seq data were performed on PCs enriched from WT and IRKO mouse kidneys as shown in Fig. 3. (C) Representative western blot probed for IR β , P-p65 Nf κ B (ser536), and GAPDH in noninfected and UPEC-infected PCs from WT and IRKO mice. Densitometry was performed to measure relative target abundance from four independent experiments and is shown in *SI Appendix, Fig. S10*.

despite having comparable IR expression to WT PCs (Fig. 7C and *SI Appendix, Fig. S10*).

IR Deletion Impacts Communication Between ICs and PCs to Dampen Immune Responses. Given these findings, we interrogated whether ICs and PCs communicate to coordinate UTI defenses. We postulated that ICs express ligands that activate PC receptors. To map these connections, we accessed iTALK to identify cognate ligand and receptor pairs expressed by ICs and PCs (30, 31). The top 20 predicted ligand–receptor pairs were plotted in WT and IRKO kidneys. We also evaluated ligand–receptor pairs categorized as “cytokines” to gauge potential IC and PC communication in immune defenses (*SI Appendix, Fig. S11*). These results illustrate intercellular communications and reveal differences in receptor–ligand interactions between WT and IRKO cells.

We then used iTALK to investigate how IR deletion rewires IC and PC communication. This analysis predicts how ligand–receptor interactions change with IR deletion (i.e., directionality). Compared to WT mice, this analysis predicted the top 20 differentially expressed ligand–receptor interactions are suppressed in IRKO

mice. When restricted to cytokines, we observed suppressed ligand–receptor interactions between ICs and PCs, indicating that IR deletion impacts immune signaling between ICs and PCs (*SI Appendix, Fig. S11*).

To identify ligands produced by ICs that activate Nf κ B in PCs, we quantified a selection of proteins in culture media isolated from WT and IRKO ICs. We measured the concentrations of twelve cytokines predicted to be suppressed in IRKO ICs and whose cognate receptors are expressed in PCs (*SI Appendix, Tables S1 and S3*). Additionally, we quantified ribonuclease 4 (RNase 4) and lipocalin 2 (Lcn 2), two AMPs regulated by IR (6). In media collected from noninfected IRKO ICs, we detected suppressed concentrations of interleukin 33 (IL-33), Lcn 2, RNase 4, and tumor necrosis factor alpha (TNF α). Following UPEC challenge, we measured suppressed concentrations of interleukin 17A (IL-17A), IL-33, Lcn 2, RNase 4, and TNF α in IRKO media (Fig. 8A and *SI Appendix, Table S4*). To test whether these proteins activate Nf κ B, we stimulated PCs with recombinant IL-17A, IL-33, Lcn 2, RNase 4, and TNF α . Western blot shows that these proteins individually can activate Nf κ B within 5 min and sustain activation at 4 h for all

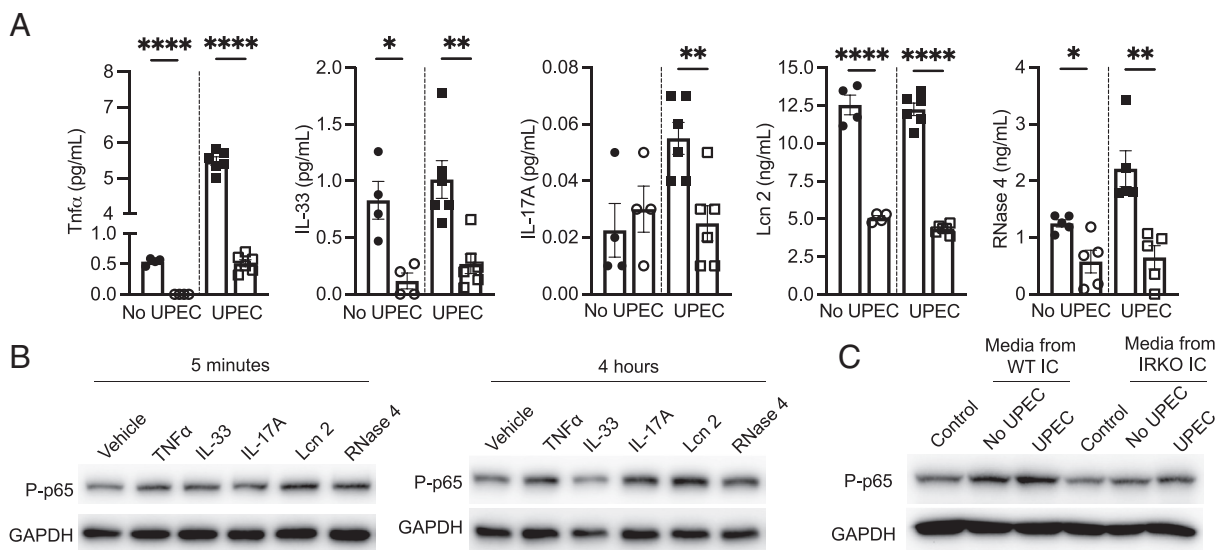


Fig. 8. ICs and PCs communicate to engage immune responses. (A) Concentrations of TNF α , IL-33, IL-17A, Lcn 2, and RNase 4 in conditioned media isolated from WT ICs (closed shapes) and IRKO ICs (open shapes) before and after UPEC infection. Graphs show the mean concentration and SEM. Asterisks denote significant *P* values for the pairwise comparison (Student's *t* test). **P* < 0.05, ***P* < 0.01, and *****P* < 0.0001. (B) Representative western blot probed for P-p65 Nf κ B (ser536) and GAPDH in PCs stimulated for 5 min (Left) or 4 h (Right) with 5 ng/mL recombinant murine TNF α , IL-33, IL-17A, Lcn 2, or RNase 4. (C) Representative western blot probed for P-p65 Nf κ B (ser536) and GAPDH in noninfected PCs (control) or PCs incubated for 1 h in conditioned media isolated from noninfected WT and IRKO ICs (no UPEC) or UPEC-infected WT and IRKO ICs (UPEC).

molecules besides IL-33 (Fig. 8B). To validate that IC cytokine production affects PC NFkB signaling, we collected conditioned media from noninfected and UPEC-challenged WT ICs and added it to PCs. The addition of conditioned media from ICs augmented PC NFkB p65 phosphorylation but media from IRKO ICs did not (Fig. 8C). These data support our hypothesis that ICs produce ligands to engage NFkB and IR deletion suppresses their expression to diminish NFkB responses in PCs.

Diabetic Mice Have Suppressed IR Targets. To assess whether the findings in IRKO mice translate to diabetic rodents, we transurethraly infected diabetic *ob/ob* and nondiabetic *ob/+* mice with UPEC (SI Appendix, Table S5). Twenty-four hours after infection, kidneys from *ob/ob* mice had greater bacterial titers (Fig. 9A). When we MACS-enriched IC and PC populations in *ob/ob* and *ob/+* kidneys, we similarly detected suppressed IR, eIF2, and NFkB expression in ICs and suppressed NFkB in PCs (Fig. 9B).

Kidneys from People with Diabetes Have Suppressed IR Targets.

To determine whether these findings translate to humans, we accessed single-nuclei RNA-seq (snRNA-seq) data from three published studies of humans with and without diabetic kidney disease (SI Appendix, Table S6) (32–34). In total, we collected data from 58,193 cells, including 4,219 ICs and 4,232 PCs (SI Appendix, Fig. S12). When we examined cell-specific gene expression changes, we identified suppressed IR, eIF2, and NFkB expression in diabetic ICs and reduced NFkB in diabetic PCs (Fig. 9C).

Discussion

This study uses preclinical models and human data to establish the importance of IR in orchestrating kidney immune responses. Our primary outcomes demonstrate IR is essential for activating integrated stress response regulators, notably ATF4, and downstream NFkB targets crucial to prevent infection. Meanwhile, our secondary outcomes show that IR deletion suppresses IC cytokine and

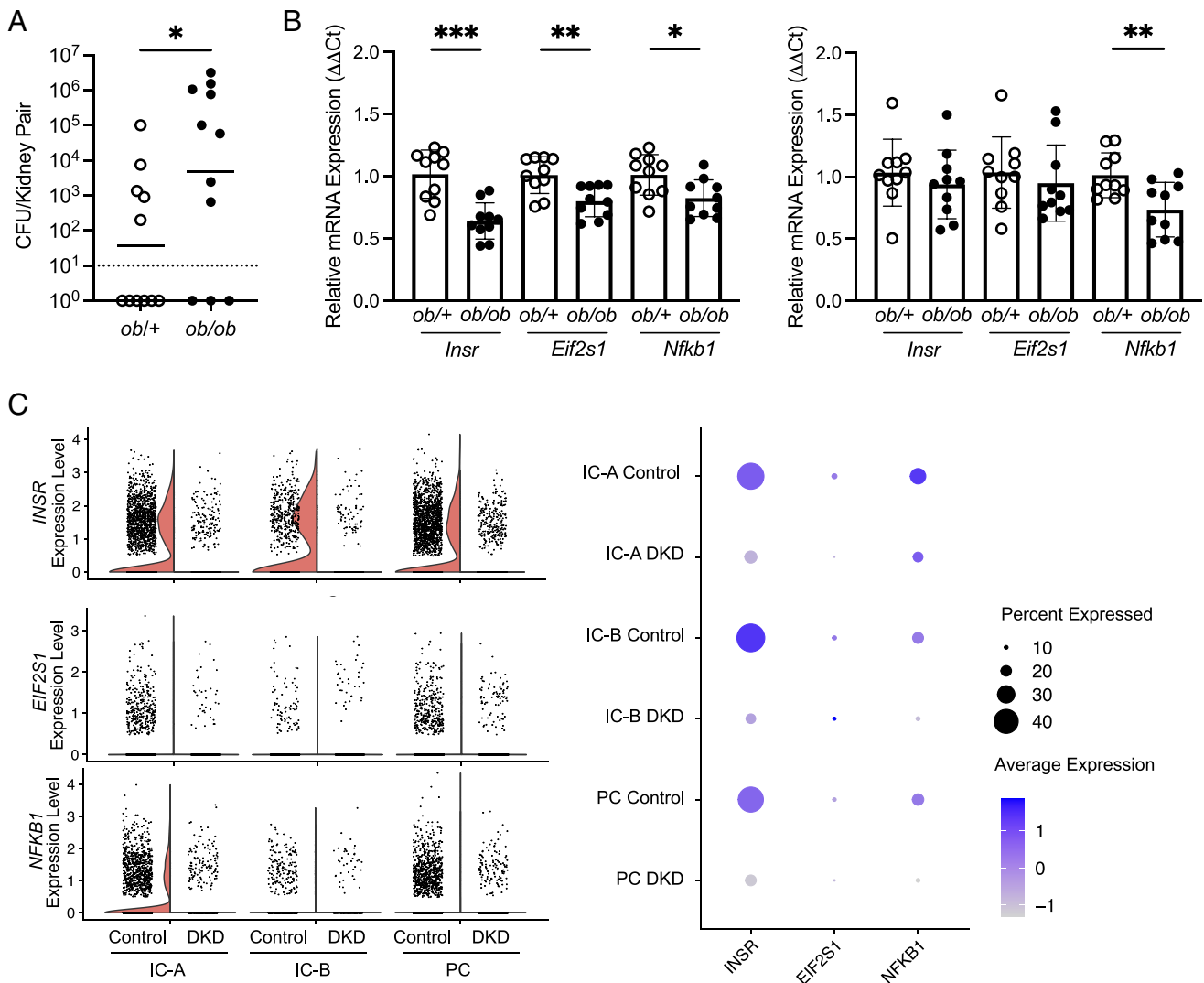


Fig. 9. The integrated stress response is suppressed in global diabetes. (A) Nondiabetic *ob/+* and diabetic *ob/ob* female mice were transurethraly infected with UPEC. Twenty-four hours after infection, UPEC were enumerated in the kidneys. Each point shows mean kidney pair UPEC burden from a separate mouse ($n = 11$ mice/genotype). The solid horizontal lines indicate the geometric means of each group. The dotted horizontal line indicates the limit of detection. The asterisk denotes significance for the indicated pairwise comparison (Mann-Whitney *U* test). (B) Relative *Insr*, *Nfkb1*, and *Eif2s1* expression in MACS-enriched ICs (Left) and PCs (Right) from noninfected female *ob/+* and *ob/ob* mice ($n = 10$ mice/genotype). Graphs show the mean expression and SEM. Asterisks denote significant *P* values for the pairwise comparison (Student's *t* test). * $P < 0.05$, ** $P < 0.01$, and **** $P < 0.0001$. (C) Available kidney snRNA-seq and scRNA-seq data were accessed from three published studies of people with and without diabetes (32–34). Violin plots (Left) and dot plots (Right) showing the expression of IR and integrated stress response genes in IC and PC clusters shown in SI Appendix, Fig. S12 from nondiabetic (control) and diabetic kidneys (DKD). Dot size indicates the percentage of cells expressing marker genes, and the color represents the average gene expression value (Right). Human subject information can be found in SI Appendix, Table S6. * $P < 0.05$, ** $P < 0.01$, and **** $P < 0.001$.

AMP expression, reprograms IC–PC communication, and shifts PC transcriptomes. These data reveal two distinct IR-mediated mechanisms that activate NFkB within the collecting duct. In ICs, intact IR and ATF4 signaling are necessary to engage NFkB. In PCs, NFkB regulation occurs through paracrine communication with ICs, where NFkB in PCs is activated by factors secreted by ICs. The significance of these findings is strengthened in diabetic rodents and using human sc-RNAseq data showing that these targets are suppressed in diabetic kidneys. Together, these outcomes identify the IR–ATF4–NFkB axis as a contributor to IC antibacterial defenses and provide initial evidence that ICs and PCs communicate to prevent infection. These insights not only shed light on the heightened UTI risk in individuals with diabetes but may also offer insight into why other insulin-resistant conditions amplify infection risk—including pregnancy, sustained inflammatory states like recurrent infections, obesity, and aging (35).

The IRKO model provides a powerful approach to dissect insulin's functions. In the kidney, IR deletion in podocytes potentiates albuminuria, IR deletion in proximal tubules affects gluconeogenesis, and IR deletion in the distal nephron and/or collecting duct impacts sodium reabsorption, vascular resistance, and blood pressure regulation (8, 36–41). Here, we demonstrate IR is necessary to oppose UPEC infection. Together, these data suggest that IR is an essential modulator of fundamental kidney processes, including immune responses. Complementary to our results, published data suggest that IR shapes host defenses in other organs. IR deletion in intestinal Paneth cells suppresses AMP expression, IR-deficient macrophages show reduced responsiveness to pathogens and have suppressed cytokine production, and T cells lacking IR exhibit reduced protective immunity against influenza (42–45). Together, these data suggest that IR is an essential modulator of cellular metabolism and fundamental biological processes, including immune responses.

In the present study, we reveal that IR deletion dampens integrated stress responses. Over the last decade, a body of evidence has uncovered a role for the integrated stress response in antimicrobial defenses—by regulating autophagy, cytokine and AMP expression, activating pattern recognition receptors, and enforcing epithelial barriers that prevent infection (46–52). Here, we establish the essential role of the IR–ATF4 pathway in the activation of NFkB. Previous research has explored the interplay between ATF4 and NFkB, and our findings align with existing experimental evidence indicating that integrated stress responses play a pivotal role in NFkB activation. Although the precise mechanisms integrated stress responses employ to activate NFkB remain undefined, lowered concentrations of IκBα, a negative NFkB regulator, is a potential etiology (24–27). Ongoing research is investigating ATF4 mechanisms contributing to NFkB activation and UTI defenses.

Limited data indicate that collecting duct cells facilitate UPEC clearance via NFkB-activated mechanisms (9, 10, 53). We show that NFkB prevents infection and modulates cytokines and AMPs. Like prior studies, we show that NFkB regulates Lcn 2, which sequesters iron needed for UPEC replication (11, 54, 55). Additionally, we provide evidence that NFkB controls RNase 4 and RNase 7 expression, which kill UPEC by compromising their membranes (56, 57). Identifying mechanisms to boost AMP production with NFkB-directed agonists may reveal therapeutic approaches for recurrent or severe infections.

While a body of work investigates IC antimicrobial defenses, limited evidence substantiates a role for PCs in UTI defense. Data suggest that PCs control immunity through the vasopressin receptor type 2 (V2R) as the V2R agonist diamino-8-D-arginine vasopressin suppresses chemokine secretion, neutrophil recruitment, and augments UPEC susceptibility (58). Here, we show that PCs

respond to UPEC by engaging NFkB. Unexpectedly, our data suggest that NFkB in PCs is dependent on secreted factors produced by ICs. This study provides evidence that ICs and PCs communicate to engage UTI defenses.

A strength of this study is the complementary use of murine models, unbiased limiting-cell RNA-seq, functional *in vitro* cultures, and available human single-cell transcriptomes to elucidate how IR orchestrates kidney epithelial UTI defenses. Importantly, our preclinical findings translate to humans as the IR-integrated stress response pathway is disrupted in diabetic ICs and NFkB is suppressed in diabetic PCs. However, this study has limitations. Because IRKO mice are on a C57BL/6 background, they are resistant to pyelonephritis (6, 59, 60). To overcome this limitation, we developed IC and PC cultures to uncover how these cells contribute to UTI defense and test how IR impacts their immunity. While we validated that low-passage ICs and PCs express lineage selective markers, it is not clear how IC and PC populations reflect mixed populations in the kidney or how these *in vitro* models resemble the *in vivo* environment. In part, we address this concern using human kidney medullary epithelial cell cultures that may more accurately reflect the heterogeneous cellular makeup of the kidney and employ *in vivo* models. Finally, while the challenge of defining crosstalk between the two cell types is not fully met by *in vitro* models, our findings provide the initial step toward understanding IC–PC communication in UTI defense. These limitations highlight why new models are needed.

To conclude, this study identifies IR as an important regulator of kidney epithelial defenses and provides evidence that IR-regulated nodes, including ATF4 and NFkB, modulate IC susceptibility to UPEC. Moreover, this study demonstrates that ICs and PCs communicate to prevent UTI. Together, these findings elucidate a critical role for the IR–ATF4–NFkB pathway in kidney antimicrobial defenses.

Materials and Methods

Materials. Details of the mice and reagents used can be found in *SI Appendix, Table S7*.

Mice. Mouse experiments were conducted in compliance with the rules and regulations of the Institutional Animal Care and Use Committee. All mice were kept under controlled temperature and humidity conditions, with a 12-h light and dark cycle, and had unrestricted access to standard rodent chow and water. Female *ob/ob*, *ob/+* controls, and C3H/HeOJ mice were purchased from Jackson Laboratory (Bar Harbor, ME). IRKO mice were generated by crossing mice homozygous for the floxed *Insr* gene with *Atp6v1b1-Cre* expressing mice (20, 61). *Atp6v1b1-Cre^{+/+};IR^{fl/fl}* progeny were then bred with *IR^{fl/fl}* mice, generating *Atp6v1b1-Cre^{+/-};IR^{fl/fl}* offspring. The Cre-dependent tdTomato (tdT) reporter was incorporated into our breeding scheme as published (6). WT IC mice were generated by crossing *Atp6v1b1-Cre* mice with tdT reporter mice. Mice were genotyped according to published protocols (6, 20). Genotyping primers are listed in *SI Appendix, Table S8*.

Mouse OSI-906 Treatment. Female C3H/HeOJ mice were enterally administered two doses of vehicle (tartaric acid) or 60 mg/kg OSI-906 (Selleckchem, Houston, TX). OSI-906 dosing was based on published data (17).

Mouse Glucose Measurements. Blood glucose concentrations were obtained with the AlphaTrak glucose monitoring system (Abbott Point of Care, Abbott Park, IL). Urinary glucose concentrations were assessed by dipstick urinalysis (Chemstrip 2 GP, Roche, Basel, Switzerland).

Mouse Infections. Female mice were infected by transurethral catheterization or the direct bladder inoculation method with 10^7 colony-forming units of UPEC strain CFT073 (6, 62). Twenty-four hours after infection, mice were anesthetized and killed. Kidneys were aseptically harvested, and UPEC were enumerated.

Mouse IC and PC Enrichment. Mouse kidneys were dissociated using the TissueLyser II (Qiagen, Hilden, Germany), digested with Collagenase IV (Thermo Fisher Scientific, Waltham, MA), and cell suspensions were passed through a 70- μ m strainer. Red cell lysis was performed, and cells were passed through a 40- μ m strainer. ICs and PCs were enriched using FACS or MACS following established protocols (6, 13, 14). **FACS:** ICs and PCs were enriched on a BD™ FACS Vantage with DiVa option cell sorter (Becton Dickinson, CA) by sorting single events consisting of tdT expressing ICs and PCs labeled with FITC-conjugated DBA lectin. Dual-labeled positive cells, representing 0.34% of the total cell population, were excluded (SI Appendix, Fig. S2) (6). **MACS:** Live cells were selected using a dead cell removal kit (Miltenyi Biotec, Bergisch Gladbach, Germany). CD45⁺ immune cells were removed using anti-mouse CD45 microbeads (Miltenyi Biotec). ICs and PCs were enriched using anti-mouse CD117 microbeads or a biotinylated DBA lectin and anti-biotin microbeads, respectively (Miltenyi Biotec) (14).

Mouse RNA Extraction and Sequencing. RNA was extracted from FACS-enriched ICs and PCs from five WT and IRKO mice using the NucleoSpin RNA Plus XS Kit (Takara Bio, San Jose, CA). Samples with RNA integrity scores³⁷, measured using the Agilent 2100 Bioanalyzer with RNA pico chip (Agilent, Carlsbad, CA), were used for sequencing. Limiting-cell RNA-seq was employed, which optimizes the signal-to-noise ratio of genes called by RNA-seq in samples consisting of limited cell numbers (63). RNA was preamplified using the Clontech SMARTer v4 kit (Takara Bio, Kusatsu, Japan), and RNA-seq libraries were generated with the Nextera XT DNA Library Prep Kit (Illumina, Inc., San Diego, CA). Samples were sequenced to a depth of 15 to 20 million paired-end (2 × 150 base pair) clusters on the Illumina HiSeq 4000 platform. Data processing and analysis are outlined in SI Appendix, Supplemental Methods. The sequences and metadata reported in this paper are deposited in the Gene Expression Omnibus (GEO) database (Accession No. GSE213985).

Human Single-Cell Transcriptomes. We accessed published human kidney snRNA-seq and scRNA-seq libraries from people with and without diabetes (GEO Accession No. GSE131882 and GSE195460) (32–34). These libraries encompassed five diabetic kidneys and nine nondiabetic kidneys. Data processing and analysis are outlined in SI Appendix, Supplemental Methods.

Cell Culture. FACS-enriched murine tdT⁺ ICs and DBA-labeled PCs were cultured in 5 μ g/mL insulin containing Renalife media (Lifeline Cell Technology, Frederick, MD). Primary human medullary kidney epithelial cells (Lifeline Cell Technology) were cultured in insulin containing Renalife complete media (64). Cells were used within four passages as we observed loss of lineage-specific markers in mouse and human cells after six passages. Transfection experiments were initiated when cells approached confluency as outlined in SI Appendix, Supplemental Methods. For UPEC infection, cells were challenged with CFT073 at 10 multiplicity of infection (MOI). UPEC attachment and invasion assays were performed as outlined in SI Appendix, Supplemental Methods (56, 65). For cellular crosstalk studies, conditioned medium was transferred directly from ICs to PCs following UPEC challenge.

qRT-PCR and Immunoblot. Cells and mouse tissues dedicated for qRT-PCR were extracted in RLT-Plus buffer (Qiagen, Hilden, Germany). Cells and mouse tissues used for western blot were lysed in 62.5 mM Tris, 2% SDS, 10% glycerol, and 5% β -mercaptoethanol and boiled for 10 min. qRT-PCR and western blot were performed as published using reagents and primers listed in SI Appendix, Tables S7 and S8 (56). Mouse Antibacterial Response PCR Arrays (Qiagen, catalog number: PAMM-148Z) were used following the manufacturer's instructions and analyzed with Qiagen's GeneGlobe Data Analysis Center. Samples were normalized to

the average geometric mean of internal controls *Actb*, *B2m*, *Gapdh*, *Gusb*, and *Hsp90ab1*. Western blots were imaged on ChemiDoc MP (Bio-Rad Laboratories, Hercules, CA). Densitometry was performed using ImageLab software, and adjusted volume band intensity values for target proteins were normalized to corresponding adjusted volume band intensity values for GAPDH. Values were plotted as mean fold change over controls \pm SEM.

Immunofluorescent Staining. Immunofluorescent staining of mouse kidneys was performed as described (6, 56). PCs were labeled with a polyclonal goat aquaporin-2 antibody or a DBA-fluorescein conjugate. TdT-positive ICs were labeled with a rabbit polyclonal RFP/tdTomato antibody, a rabbit polyclonal AE1 antibody, or a rabbit monoclonal ATP6V1B1 antibody. Alexa Fluor® 488 AffiniPure Donkey Anti-Goat IgG and Cy™3 AffiniPure F(ab)₂ Fragment Donkey Anti-Rabbit IgG served as secondary antibodies. Antibody information is described in SI Appendix, Table S7.

ELISA. Cytokines and Lcn 2 were quantified in culture media using the MESO QuickPlex SQ 120 instrument (Meso Scale Discovery Platform, Rockville, MD). RNase 4 was measured using a commercially available mouse RNase 4 ELISA (MyBioSource, San Diego, CA).

Chromatin Immunoprecipitation (ChIP). ChIP was performed using the SimpleChIP Enzymatic Chromatin IP Kit (Cell Signaling Technology, Danvers, MA). Human medullary kidney epithelial cells were cultured to near confluence and infected with CFT073 for 3 h. Chromatin was prepared according to kit instructions. Immunoprecipitation reactions included negative control rabbit IgG, positive control histone H3. Immunoprecipitation was performed using an anti-total P65 antibody (Cell Signaling). Following ChIP, real-time qPCRs were performed with primers targeting P65 peaks for *RNASE4*, *RNASE7*, and *LCN2* identified using ChIP-seq data from the encyclopedia of DNA elements (ENCODE) project (SI Appendix, Table S8) (66). Results are expressed as percent precipitated DNA compared to total input:

$$\% \text{ Precipitated DNA} = \frac{100}{2^{(C_i[\text{ChIP}] - C_i[\text{Input}] - \log_2(\text{Input Dilution Factor}))}}$$

Statistics. The D'Agostino–Pearson Omnibus or Shapiro–Wilk tests were used to assess whether datasets followed a normal distribution, with normality defined as a *P*-value > 0.05. All in vitro data exhibited a normal distribution, whereas in vivo data did not conform to a normal distribution. As indicated in the figure legends, the Student's *t* test was employed for two-way comparisons involving normally distributed data, while the nonparametric Mann–Whitney *U* test was used otherwise. Differences between groups with a *P*-value < 0.05 were regarded as statistically significant.

Data, Materials, and Software Availability. RNAseq data have been deposited in Gene Expression Omnibus (GSE213985). Previously published data were used for this work [(21, GSE119531), (32, GSE195460), (33), (34, GSE131882)].

ACKNOWLEDGMENTS. We thank Birong (Rollin) Li in the Kidney and Urinary Tract Center at the Abigail Wexner Research Institute for assistance with mouse infections. We thank Dave Dunaway in the Flow Cytometry Core at the Abigail Wexner Research Institute for operating the cell sorter used for FACS. This work is supported by the NIH (NIDDK) R01 DK114035 and R01 DK115737 (J.D.S.). P.Y. is supported by National Cancer Institute R50CA211524. Limiting-cell RNA-seq was performed at The Ohio State University Comprehensive Cancer Center's Genomics Shared Resource which is supported by a Comprehensive Cancer Support Grant P30CA016058.

- O. Nitzan, M. Elias, B. Chazan, W. Saliba, Urinary tract infections in patients with type 2 diabetes mellitus: Review of prevalence, diagnosis, and management. *Diabetes Metab. Syndr. Obes.* **8**, 129–136 (2015).
- B. R. Shah, J. E. Hux, Quantifying the risk of infectious diseases for people with diabetes. *Diabetes Care* **26**, 510–513 (2003).
- L. M. Muller *et al.*, Increased risk of common infections in patients with type 1 and type 2 diabetes mellitus. *Clin. Infect. Dis.* **41**, 281–288 (2005).
- S. Kumar *et al.*, Acute pyelonephritis in diabetes mellitus: Single center experience. *Indian J. Nephrol.* **24**, 367–371 (2014).
- B. Kim *et al.*, Diabetes mellitus increases mortality in acute pyelonephritis patients: A population study based on the National Health Insurance Claim Data of South Korea for 2010–2014. *Infection* **48**, 435–443 (2020).

- M. J. Murtha *et al.*, Insulin receptor signaling regulates renal collecting duct and intercalated cell antibacterial defenses. *J. Clin. Invest.* **128**, 5634–5646 (2018).
- J. Boucher, A. Kleinridders, C. R. Kahn, Insulin receptor signaling in normal and insulin-resistant states. *Cold Spring Harb. Perspect. Biol.* **6**, 1–23 (2014).
- L. J. Hale, R. J. Coward, The insulin receptor and the kidney. *Curr. Opin. Nephrol. Hypertens* **22**, 100–106 (2013).
- L. Schwartz, J. de Dios Ruiz-Rosado, E. Stonebrook, B. Becknell, J. D. Spencer, Uropathogen and host responses in pyelonephritis. *Nat. Rev. Nephrol.* **19**, 658–671 (2023), 10.1038/s41581-023-00737-6.
- C. Chassin *et al.*, Renal collecting duct epithelial cells react to pyelonephritis-associated *Escherichia coli* by activating distinct TLR4-dependent and -independent inflammatory pathways. *J. Immunol.* **177**, 4773–4784 (2006).

11. N. Paragas *et al.*, alpha-Intercalated cells defend the urinary system from bacterial infection. *J. Clin. Invest.* **124**, 2963–2976 (2014).
12. C. Chassin, E. Tourneur, M. Bens, A. Vandewalle, A role for collecting duct epithelial cells in renal antibacterial defences. *Cell. Microbiol.* **13**, 1107–1113 (2011).
13. V. Saxena *et al.*, Whole transcriptome analysis of renal intercalated cells predicts lipopolysaccharide mediated inhibition of retinoid X receptor alpha function. *Sci. Rep.* **9**, 545 (2019).
14. V. Saxena *et al.*, Kidney intercalated cells are phagocytic and acidify internalized uropathogenic *Escherichia coli*. *Nat. Commun.* **12**, 2405 (2021).
15. V. Saxena *et al.*, Cell specific qRT-PCR of renal epithelial cells reveals a novel innate immune signature in murine collecting duct. *Am. J. Physiol. Renal Physiol.* **315**, F812–F823 (2017), 10.1152/ajprenal.00512.2016.
16. B. Becknell, A. Schwaderer, D. S. Hains, J. D. Spencer, Amplifying renal immunity: The role of antimicrobial peptides in pyelonephritis. *Nat. Rev. Nephrol.* **11**, 642–655 (2015).
17. M. J. Mulvihill *et al.*, Discovery of OSI-906: A selective and orally efficacious dual inhibitor of the IGF-1 receptor and insulin receptor. *Future Med. Chem.* **1**, 1153–1171 (2009).
18. B. Li *et al.*, Inflammation drives renal scarring in experimental pyelonephritis. *Am. J. Physiol. Renal Physiol.* **312**, F43–F53 (2017).
19. A. J. Carey *et al.*, Urinary tract infection of mice to model human disease: Practicalities, implications and limitations. *Crit. Rev. Microbiol.* **42**, 780–799 (2016).
20. R. L. Miller *et al.*, The V-ATPase B1-subunit promoter drives expression of Cre recombinase in intercalated cells of the kidney. *Kidney Int.* **75**, 435–439 (2009).
21. H. Wu, Y. Kiritia, E. L. Donnelly, B. D. Humphreys, Advantages of single-nucleus over single-cell RNA sequencing of adult kidney: Rare cell types and novel cell states revealed in fibrosis. *J. Am. Soc. Nephrol.* **30**, 23–32 (2019).
22. P. D. Olson, K. A. Hruska, D. A. Hunstad, Androgens enhance male urinary tract infection severity in a new model. *J. Am. Soc. Nephrol.* **27**, 1625–1634 (2016).
23. L. Chen *et al.*, Transcriptomes of major renal collecting duct cell types in mouse identified by single-cell RNA-seq. *Proc. Natl. Acad. Sci. U.S.A.* **114**, E9989–E9998 (2017).
24. M. Costa-Mattoli, P. Walter, The integrated stress response: From mechanism to disease. *Science* **368**, eaat5314 (2020).
25. J. Deng *et al.*, Translational repression mediates activation of nuclear factor kappa B by phosphorylated translation initiation factor 2. *Mol. Cell Biol.* **24**, 10161–10168 (2004).
26. R. C. Wek, Role of eIF2alpha kinases in translational control and adaptation to cellular stress. *Cold Spring Harb. Perspect. Biol.* **10**, a032870 (2018).
27. H. Y. Jiang, R. C. Wek, Phosphorylation of the alpha-subunit of the eukaryotic initiation factor-2 (eIF2alpha) reduces protein synthesis and enhances apoptosis in response to proteasome inhibition. *J. Biol. Chem.* **280**, 14189–14202 (2005).
28. M. Boyce *et al.*, A selective inhibitor of eIF2alpha dephosphorylation protects cells from ER stress. *Science* **307**, 935–939 (2005).
29. H. P. Harding, Y. Zhang, D. Ron, Protein translation and folding are coupled by an endoplasmic-reticulum-resident kinase. *Nature* **397**, 271–274 (1999).
30. Y. E. A. Wang, iTALK: An R package to characterize and illustrate intercellular communication. bioRxiv [Preprint] (2019), <https://doi.org/10.1101/507871> (Accessed 15 January 2024).
31. E. Armingol, A. Officer, O. Harismendy, N. E. Lewis, Deciphering cell-cell interactions and communication from gene expression. *Nat. Rev. Genet.* **22**, 71–88 (2021).
32. P. C. Wilson *et al.*, Multimodal single cell sequencing implicates chromatin accessibility and genetic background in diabetic kidney disease progression. *Nat. Commun.* **13**, 5253 (2022).
33. P. C. Wilson *et al.*, The single-cell transcriptomic landscape of early human diabetic nephropathy. *Proc. Natl. Acad. Sci. U.S.A.* **116**, 19619–19625 (2019).
34. Y. Muto *et al.*, Single cell transcriptional and chromatin accessibility profiling redefine cellular heterogeneity in the adult human kidney. *Nat. Commun.* **12**, 2190 (2021).
35. B. Foxman, Epidemiology of urinary tract infections: Incidence, morbidity, and economic costs. *Am. J. Med.* **113**, 5S–13S (2002).
36. S. Tiwari *et al.*, Deletion of the insulin receptor in the proximal tubule promotes hyperglycemia. *J. Am. Soc. Nephrol.* **24**, 1209–1214 (2013).
37. G. Pandey *et al.*, Reduced insulin receptor expression enhances proximal tubule gluconeogenesis. *J. Cell Biochem.* **118**, 276–285 (2017).
38. L. Li *et al.*, Reduced ENaC activity and blood pressure in mice with genetic knockout of the insulin receptor in the renal collecting duct. *Am. J. Physiol. Renal Physiol.* **304**, F279–288 (2013).
39. S. Tiwari *et al.*, Impaired sodium excretion and increased blood pressure in mice with targeted deletion of renal epithelial insulin receptor. *Proc. Natl. Acad. Sci. U.S.A.* **105**, 6469–6474 (2008).
40. G. I. Welsh *et al.*, Insulin signaling to the glomerular podocyte is critical for normal kidney function. *Cell Metab.* **12**, 329–340 (2010).
41. M. Nakamura *et al.*, Insulin promotes sodium transport but suppresses gluconeogenesis via distinct cellular pathways in human and rat renal proximal tubules. *Kidney Int.* **97**, 316–326 (2020).
42. S. F. Andres *et al.*, Deletion of intestinal epithelial insulin receptor attenuates high-fat diet-induced elevations in cholesterol and stem, enteroendocrine, and Paneth cell mRNAs. *Am. J. Physiol. Gastrointest. Liver Physiol.* **308**, G100–111 (2015).
43. S. Tsai *et al.*, Insulin receptor-mediated stimulation boosts T cell immunity during inflammation and infection. *Cell Metab.* **28**, 922–934 e924 (2018).
44. T. Senokuchi *et al.*, Forkhead transcription factors (FoxOs) promote apoptosis of insulin-resistant macrophages during cholesterol-induced endoplasmic reticulum stress. *Diabetes* **57**, 2967–2976 (2008).
45. E. Ieronymaki *et al.*, Insulin resistance in macrophages alters their metabolism and promotes an M2-like phenotype. *J. Immunol.* **202**, 1786–1797 (2019).
46. A. Bretin *et al.*, Activation of the EIF2AK4-EIF2A/eIF2alpha-ATF4 pathway triggers autophagy response to Crohn disease-associated adherent-invasive *Escherichia coli* infection. *Autophagy* **12**, 770–783 (2016).
47. Y. Iwasaki *et al.*, Activating transcription factor 4 links metabolic stress to interleukin-6 expression in macrophages. *Diabetes* **63**, 152–161 (2014).
48. D. Vasudevan *et al.*, The GCN2-ATF4 signaling pathway induces 4E-BP to bias translation and boost antimicrobial peptide synthesis in response to bacterial infection. *Cell Rep.* **21**, 2039–2047 (2017).
49. X. Hu *et al.*, ATF4 deficiency promotes intestinal inflammation in mice by reducing uptake of Glutamine and expression of antimicrobial peptides. *Gastroenterology* **156**, 1098–1111 (2019).
50. I. Tattoli *et al.*, Amino acid starvation induced by invasive bacterial pathogens triggers an innate host defense program. *Cell Host Microbe* **11**, 563–575 (2012).
51. L. Rodrigues, R. S. F. Graca, L. A. M. Carneiro, Integrated stress responses to bacterial pathogenesis patterns. *Front. Immunol.* **9**, 1306 (2018).
52. C. Zhang *et al.*, ATF4 is directly recruited by TLR4 signaling and positively regulates TLR4-triggered cytokine production in human monocytes. *Cell Mol. Immunol.* **10**, 84–94 (2013).
53. C. Kuper, F. X. Beck, W. Neuhof, Toll-like receptor 4 activates NF-kappaB and MAP kinase pathways to regulate expression of proinflammatory COX-2 in renal medullary collecting duct cells. *Am. J. Physiol. Renal Physiol.* **302**, F38–46 (2012).
54. M. Steigedal *et al.*, Lipocalin 2 imparts selective pressure on bacterial growth in the bladder and is elevated in women with urinary tract infection. *J. Immunol.* **193**, 6081–6089 (2014).
55. J. B. Cowland, O. E. Sorensen, M. Sehested, N. Borregaard, Neutrophil gelatinase-associated lipocalin is up-regulated in human epithelial cells by IL-1 beta, but not by TNF-alpha. *J. Immunol.* **171**, 6630–6639 (2003).
56. K. Bender *et al.*, Expression and function of human ribonuclease 4 in the kidney and urinary tract. *Am. J. Physiol. Renal Physiol.* **320**, F972–F983 (2021).
57. J. D. Spencer *et al.*, Ribonuclease 7, an antimicrobial peptide upregulated during infection, contributes to microbial defense of the human urinary tract. *Kidney Int.* **83**, 615–625 (2013).
58. C. Chassin *et al.*, Hormonal control of the renal immune response and antibacterial host defense by arginine vasopressin. *J. Exp. Med.* **204**, 2837–2852 (2007).
59. W. J. Hopkins, A. Gendron-Fitzpatrick, E. Balish, D. T. Uehling, Time course and host responses to *Escherichia coli* urinary tract infection in genetically distinct mouse strains. *Infect. Immun.* **66**, 2798–2802 (1998).
60. T. J. Hannan, I. U. Mysorekar, C. S. Hung, M. L. Isaacson-Schmid, S. J. Hultgren, Early severe inflammatory responses to uropathogenic *E. coli* predispose to chronic and recurrent urinary tract infection. *PLoS Pathog.* **6**, e1001042 (2010).
61. J. C. Bruning *et al.*, A muscle-specific insulin receptor knockout exhibits features of the metabolic syndrome of NIDDM without altering glucose tolerance. *Mol. Cell* **2**, 559–569 (1998).
62. P. D. Olson *et al.*, Androgen exposure potentiates formation of intratubular communities and renal abscesses by *Escherichia coli*. *Kidney Int.* **94**, 502–513 (2018).
63. L. A. Walker *et al.*, CLEAR: Coverage-based limiting-cell experiment analysis for RNA-seq. *J. Transl. Med.* **18**, 63 (2020).
64. T. E. Eichler *et al.*, Insulin and the phosphatidylinositol 3-kinase signaling pathway regulate Ribonuclease 7 expression in the human urinary tract. *Kidney Int.* **90**, 568–579 (2016).
65. T. Eichler *et al.*, Ribonuclease 7 shields the kidney and bladder from invasive uropathogenic *Escherichia coli* infection. *J. Am. Soc. Nephrol.* **30**, 1385–1397 (2019).
66. K. R. Rosenbloom *et al.*, ENCODE data in the UCSC genome browser: Year 5 update. *Nucleic Acids Res.* **41**, D56–63 (2013).